One-dimensional Bose gas on an atom chip

van Amerongen, A.H.

6 Yang-Yang thermodynamics on an atom chip

In this chapter we describe measurements on the behavior of a weakly interacting nearly one-dimensional (1D) trapped Bose gas at finite temperature. We perform *in situ* measurements of spatial density profiles and show that they are very well described by a model based on exact solutions obtained using the Yang-Yang thermodynamic formalism, in a regime where other, approximate theoretical approaches fail. We demonstrate Bose gas focusing as a means to gain experimental access to the axial momentum distribution of the gas, and find good agreement with the *in situ* results.

6.1 Introduction

Reducing the dimensionality in a quantum system can have dramatic consequences. For example, the 1D Bose gas with repulsive delta-function interaction exhibits a surprisingly rich variety of physical regimes that is not present in 2D or 3D (see Sec. 2.6). This 1D Bose gas model is of particular interest because exact solutions for the many-body eigenstates can be obtained using a Bethe ansatz (Sec. 2.5.2). Furthermore, the finite-temperature equilibrium can be studied using the Yang-Yang thermodynamic formalism [36–38], a method also known as the thermodynamic Bethe ansatz (Sec. 2.5.3). The experimental achievement of ultracold atomic Bose gases in the 1D regime [39–41, 178] has attracted renewed attention to the 1D Bose gas problem [73, 84, 179–181] and is now providing previously unattainable opportunities to test the Yang-Yang thermodynamics.

In this chapter, we present the first direct comparison between experiments and theory based on the Yang-Yang exact solutions. The comparison is done in the weakly interacting regime and covers a wide parameter range where conventional models fail to quantitatively describe *in situ* measured spatial density profiles. Furthermore, we show that Bose gas focusing allows experimental access to the equilibrium momentum distribution of the 1D gas, which is difficult to obtain through other means.

Theory for the 1D Bose gas is summarized in Ch. 2. In brief, for a uniform 1D Bose gas, the key parameter is the dimensionless interaction strength $\gamma = mg_1/\hbar^2 n_1$, where m is the mass of the particles, n_1 is the 1D density, and g_1 is the 1D coupling

constant. An overview of the regimes in 1D is shown in Fig. 2.4. At low densities or large coupling strength such that $\gamma \gg 1$, the gas is in the strongly interacting or Tonks-Girardeau regime [42, 43, 53]. The opposite limit $\gamma \ll 1$ corresponds to the weakly interacting gas. Here, for temperatures below the temperature of quantum degeneracy $T_d = \hbar^2 n_1^2/2mk_B$, one distinguishes two regimes [59]. *(i)* For sufficiently low temperatures, $T \ll \sqrt{\gamma} T_d$, the equilibrium state is a quasi-condensate with suppressed density fluctuations and fluctuating phase. The system can be treated by the mean-field approach and by the Bogoliubov theory of excitations. The 1D character manifests itself through long-wavelength phase fluctuations resulting in a finite phase coherence length $l_\phi = \hbar^2 n_1/mk_B T$ which greatly exceeds the mean-field correlation length $l_c = \hbar/\sqrt{mn_1 g_1}$. *(ii)* The temperature interval $\sqrt{\gamma} T_d \ll T \ll T_d$ corresponds to the quantum decoherent regime [59], where both the density and the phase fluctuate. Here, the condition $l_c \ll l_\phi$ required for the existence of a quasi-condensate is no longer satisfied and the system can be treated as a degenerate ideal gas combined with perturbation theory in g_1. At temperatures near the crossover to the quasi-condensate, $T \sim \sqrt{\gamma} T_d$, neither of the above mentioned approximate theoretical approaches work and one has to rely on the numerical solution to the exact Yang-Yang equations, as we show in this chapter.

Experiments on 1D Bose gases are usually carried out in harmonic traps with strong transverse confinement and weak confinement along the symmetry axis, $\omega_\perp \gg \omega_\parallel$. A trapped gas is in the 1D regime if both temperature and chemical potential are small with respect to the radial excitation energy, $k_B T, \mu \ll \hbar\omega_\perp$. The effective 1D coupling can be expressed through the 3D scattering length a as $g_1 \simeq 2\hbar\omega_\perp a$ if $a \ll (\hbar/m\omega_\perp)^{1/2}$ [33][Eq. (2.34)]. Various physical regimes of a harmonically trapped 1D gas have been discussed in Refs. [34, 70, 76, 85]. The above classification of the regimes for the uniform gas can be applied locally to the trapped gas if the conditions for the local density approximation (LDA) are met [70, 76, 85]. It was recognized early on that the physics of the degenerate part of the trapped cloud is already effectively 1D if the weaker condition $\mu < \hbar\omega_\perp$ is satisfied [39–41, 178].

We experimentally investigate the behavior of a weakly interacting trapped Bose gas ($\gamma \approx 10^{-2}$) in the regime where $\mu < \hbar\omega_\perp$ and $k_B T \simeq \hbar\omega_\perp$. Similar measurements to our *in situ* data were previously performed at higher chemical potentials and higher temperatures [60], in which case the observed density profiles were found to be in disagreement not only with a pure quasi-condensate description and with an ideal-gas description, but also with a model based on a Hartree-Fock approximation. Our approach here is different in that we fit the data using a model based on the solutions to the exact Yang-Yang equations [36, 59] and use these fits to extract the chemical potential and the temperature of the gas. The model describes our *in situ* data very well, in contrast to the more conventional descriptions.

The outline of this chapter is as follows. In Sec. 6.2 a short summary of the used methods is given. In Sec. 6.3 and Sec. 6.4 we describe the data obtained with the *in situ* and *in focus* methods respectively. In Sec. 6.5 the presented data are discussed and compared with theory. Finally, in Sec. 6.6, we conclude this chapter and give an outlook to further experimental and theoretical investigations.

6.2 Methods

For (nearly) 1D clouds, it is difficult to obtain experimental access to the axial momentum distribution. The conventional time-of-flight method does not work for this purpose, mainly because the cloud hardly expands axially beyond its long initial length. In addition, we observe strong density fluctuations, similar to the example given in Fig. 5.7(a), that develop in time-of-flight from the initial phase fluctuations of our 1D degenerate clouds further complicating the analysis. Previous work for elongated 3D condensates with $\mu > \hbar\omega_\perp$ can be found in Refs. [171, 172]. Bragg spectroscopy has been demonstrated as a means to obtain the axial momentum distribution of phase-fluctuating condensates [172], but this requires averaging over many realizations of the experiment.

We gain experimental access to the axial momentum distribution using Bose gas focusing a technique that is described in detail in Ch.5. In brief, we apply a short, strong axial harmonic potential yielding a kick to the atoms proportional to their distance from the trap center (analogous to the action of a lens in optics), followed by free propagation. As a result the atoms come to a focus, at which time the axial density distribution reflects the axial momentum distribution before focusing. Initial phase fluctuations do not lead to density fluctuations in the focus, but instead result in a finite width of the cloud [127]. Since the focusing brings all atoms together axially, the signal level is high, even for a single realization. As we will show, averaging over a few shots is sufficient to obtain high signal-to-noise ratio.

The core of our experimental setup is a magnetic microtrap that is described in Sec. 3.3. The experimental procedure to prepare our cold atom samples is described in Ch. 4. In short, we trap 2×10^7 ^{87}Rb atoms in the $F = 2, m_F = 2$ state in a tight magnetic trap near the chip surface, and perform forced evaporative cooling by applying a radio frequency (RF) field. The frequency ω_{RF} is ramped down from 27 MHz to 1.7 MHz relatively quickly (in 180 ms) to purposely reduce the atom number. Apart from that the experimental procedure is identical to that of Ch. 5. Before reaching degeneracy we relax the axial confinement to a final trap with $\omega_\perp/2\pi = 3280$ Hz, $\omega_\parallel/2\pi = 8.5$ Hz, and a bottom corresponding to $\omega_{RF}/2\pi = 1.518(2)$ MHz. The current in the Z-wire is set at 2.25 A, and the distance of the cloud to the chip surface is 90 μm. In this trap we perform a slower ramp (450 ms) to the final RF frequency. An additional 300 ms of plain evaporation allows the damping of residual quadrupole collective oscillations in the cloud to the point where these oscillations are no longer visible.

6.3 *In situ* density profiles

In Fig. 6.1(a)-(e) we show the linear density of atomic clouds in the magnetic trap for different final RF frequencies. These data were obtained by *in situ* absorption imaging and integrating the atom number along z. The absolute atom number was calibrated using time-of-flight data. Each curve is an average of ~ 18 images taken under identical circumstances. Since all of our data was taken for $\mu < \hbar\omega_\perp$, we

expect[1] that the interactions will significantly affect only the distribution in the radial *ground* state, while the population in the radially *excited* states can to a good approximation be described by the ideal-gas distribution. This leads to the following model that was used to analyze the *in situ* data.

We start from the solution to the Yang-Yang integral equations for a finite-temperature uniform 1D Bose gas at thermal equilibrium [36]. As was shown in Sec. 2.5.3, this yields numerical results for both the equation of state $n_{YY}(\mu, T)$ and the local pair correlation function $g^{(2)}$ [59]. The local density approximation is then used to account for the axial potential via a varying chemical potential $\mu(x) = \mu - V(x)$. This approach is expected to be valid as long as the axial potential is smooth on the scale of the relevant correlation lengths [70, 85].

Our axial trapping potential was characterized with standard methods using both the measurement of *in situ* density profiles at high T [129] and the dipole mode oscillation frequency in the trap center. The curvature in the trap center corresponds to a frequency of 8.5 Hz, while for larger $|x|$ (in the wings of the warmer clouds) the curvature corresponds to a frequency of 6.4 Hz [128].

Since our temperature is on the order of the radial level splitting, $\hbar\omega_\perp/k_B = 158$ nK, the fraction of the gas which occupies radially excited states can not be neglected. We account for this fraction by summing over radially excited states [radial quantum number j, degeneracy $(j+1)$] and treating each radial state as an independent ideal 1D Bose gas in thermal equilibrium with the gas in the radial ground state, $\mu_j(x) = \mu(x) - j\hbar\omega_\perp$. Within this model the density is given by

$$n_l(x, \mu, T) = n_{YY}(\mu(x), T) + \sum\nolimits_{j=1}^{\infty} (j+1) n_e(\mu_j(x), T). \tag{6.1}$$

For the radially excited states, we use the result of the LDA for the 1D ideal gas, $n_e(\mu, T) = g_{1/2}(\exp(\mu/k_B T))/\Lambda_T$ where $g_{1/2}$ is a Bose function and $\Lambda_T = (2\pi\hbar^2/mk_BT)^{1/2}$ is the thermal de Broglie wavelength (see Sec. 2.3.2). In this model, the radially excited states act as a bath for particle and energy exchange with the radial ground state. The resulting fits are shown as solid lines in Fig. 6.1(a)-(e) and describe our data very well. The fitted values of T and μ are displayed in Fig. 6.2.

6.4 *In focus* density profiles

We now turn to the *in focus* measurements which give access to the axial momentum distribution of the gas (see Ch. 5). The focusing pulse is created in the same way as described in Sec. 5.6, by ramping up the axial trapping frequency from 8.5 Hz to 20 Hz in 0.8 ms, maintaining this for 3.8 ms, and ramping back down to 8.5 Hz in 0.8 ms. This is followed by a sudden switch-off of the magnetic trap. During the focusing pulse the cloud length reduces by less than 20%. After switching off the magnetic trap, the cloud expands in the radial direction on a timescale of $1/\omega_\perp$, so that the interactions vanish rapidly compared to the relevant axial timescale and the

[1] For our trap parameters the condition $\mu < \hbar\omega_\perp$ corresponds to $n < 3/4a \approx 150\ \mu\text{m}^{-1}$, see Sec. 2.4.3

subsequent axial contraction can be treated as free propagation. We experimentally observe that the cloud comes to an axial focus after a free propagation time of 13 ms. The focus time is reduced as compared to the measurements performed at higher linear densities that were presented in Sec. 5.6; these data could be modelled using a mean-field description. The observed earlier time of focus for the data presented here indicates the failure of the mean-field description – as was already hinted at in Sec. 5.7, Fig. 5.12 – that will be discussed in the next section.

In Fig. 6.1(f)-(i) we show the axial density distribution obtained in the focus, averaged over typically 10 shots, for final RF frequencies similar to the *in situ* data in Fig. 6.1 (a)-(e). Here, in contrast to the *in situ* results, one can clearly distinguish a narrow peak from a broad pedestal for RF values below 1.56 MHz [Figs. 6.1(h)-(j)]. The Yang-Yang solution does not yield the momentum distribution and thus it can not be used to fit to the *in focus* data. Instead, to quantify the observation of the bimodal structure we first fit a 2D Gaussian to the wings of the atomic density distribution. In a second step we fit a narrow Gaussian to the residual peak in the center. The fitted curves are shown after integration in the z direction in Fig. 6.1(f)-(j), and describe the observed *in focus* distributions well.

6.5 Analysis and discussion

Fig. 6.2(c) shows the resulting atom numbers in the wide and narrow part of the momentum distribution; we also plot the atom numbers from the Yang-Yang model in the radial ground state, in the radially excited states, and atoms in the radial ground state experiencing $\mu(x) > 0$. Comparing the *in situ* and the *in focus* data, we conclude that: *(i)* the momentum distribution becomes bimodal around the point where the global chemical potential μ crosses zero and becomes positive; and *(ii)* the narrow part of the momentum distribution is dominated by the atoms in the radial ground state (described by n_{YY}), while the wide part is dominated by atoms in the radially excited states.

A further comparison between the *in focus* and *in situ* results can be made as follows. Estimates for the temperature can be obtained from the Gaussian fit to the wide part of the *in focus* data, by assuming that the tails (where degeneracy is negligible) are well described by Boltzmann statistics. The resulting temperatures are shown in Fig. 6.2(a). The agreement with the temperature extracted from the *in situ* data is reasonable. We attribute the remaining discrepancy to the approximations implicit in the above interpretation of the Gaussian fit results, which neglects the discrete radial level structure and the contribution of the radial ground state to the wide part of the axial momentum distribution.

The failure of both the ideal-gas and quasi-condensate descriptions is illustrated in Fig. 6.1(c)-(e). The key point here is the following. The Yang-Yang thermodynamic equations yield a smooth equation of state $n_{YY}(\mu, T)$, including the region around $\mu(x) = 0$, as is plotted in Fig. 2.2. This deviates dramatically from both the ideal-gas description (diverging density as μ approaches zero from below) and the quasi-condensate description (vanishing density as μ approaches zero from above).

The region in $\mu(x)$ (and consequently in $n_{YY}(x)$) where this discrepancy is significant is particularly large for our parameters, and the Yang-Yang thermodynamic solutions are essential for a proper description of the *in situ* data. For example, for our trap parameters and $T = 140$ nK [as in Fig. 6.1(e)] the point $T = \sqrt{\gamma}T_d$ (or equivalently $l_\phi = 2l_c$) corresponds to $n_{YY} = 20\ \mu\text{m}^{-1}$. At this temperature the Yang-Yang equation of state deviates significantly from the ideal-gas and quasi-condensate description over the range $2 \lesssim n_{YY}(x) \lesssim 30\ \mu\text{m}^{-1}$ and the calculated value of the local pair correlation function $g^{(2)}$ varies smoothly between 1.1 and 1.8 in this range (see Fig. 2.2). This differs from the ideal-gas value of 2 and the quasi-condensate value of ≈ 1, and confirms the breakdown of the Hartree-Fock model of Ref. [60] which sets $g^{(2)} = 2$.

6.6 Conclusion and outlook

In conclusion, we have found excellent agreement between *in situ* measurements of the spatial linear density of a nearly 1D trapped Bose gas and a model based on the exact Yang-Yang solutions. We have measured the corresponding momentum distribution for which currently no theoretical comparison is available. We expect that these results will stimulate further theoretical and experimental studies of Yang-Yang thermodynamics. In addition, our findings should be relevant to experiments performed at similar linear densities and temperatures, such as guided-wave atom lasers [147] and atom-chip based interferometers [96].

Figure 6.1 on next page: Linear atomic density from absorption images obtained *in situ* (a)-(e) and *in focus* (f)-(j). The data from top to bottom correspond to lowering the value of the final RF evaporation frequency as indicated. *In situ*: solid black lines are fits using Yang-Yang thermodynamic equations (see text). The values of μ and T resulting from the fits are shown in the figure. Red line: ideal Bose gas profile showing divergence for $\mu = 0$. Green line in (e): quasi-condensate profile with the same peak density as the experimental data. *In focus*: blue lines are the sum of two independent Gaussian fits – one to the wings (light blue) and one to the central part of the atomic density distribution.

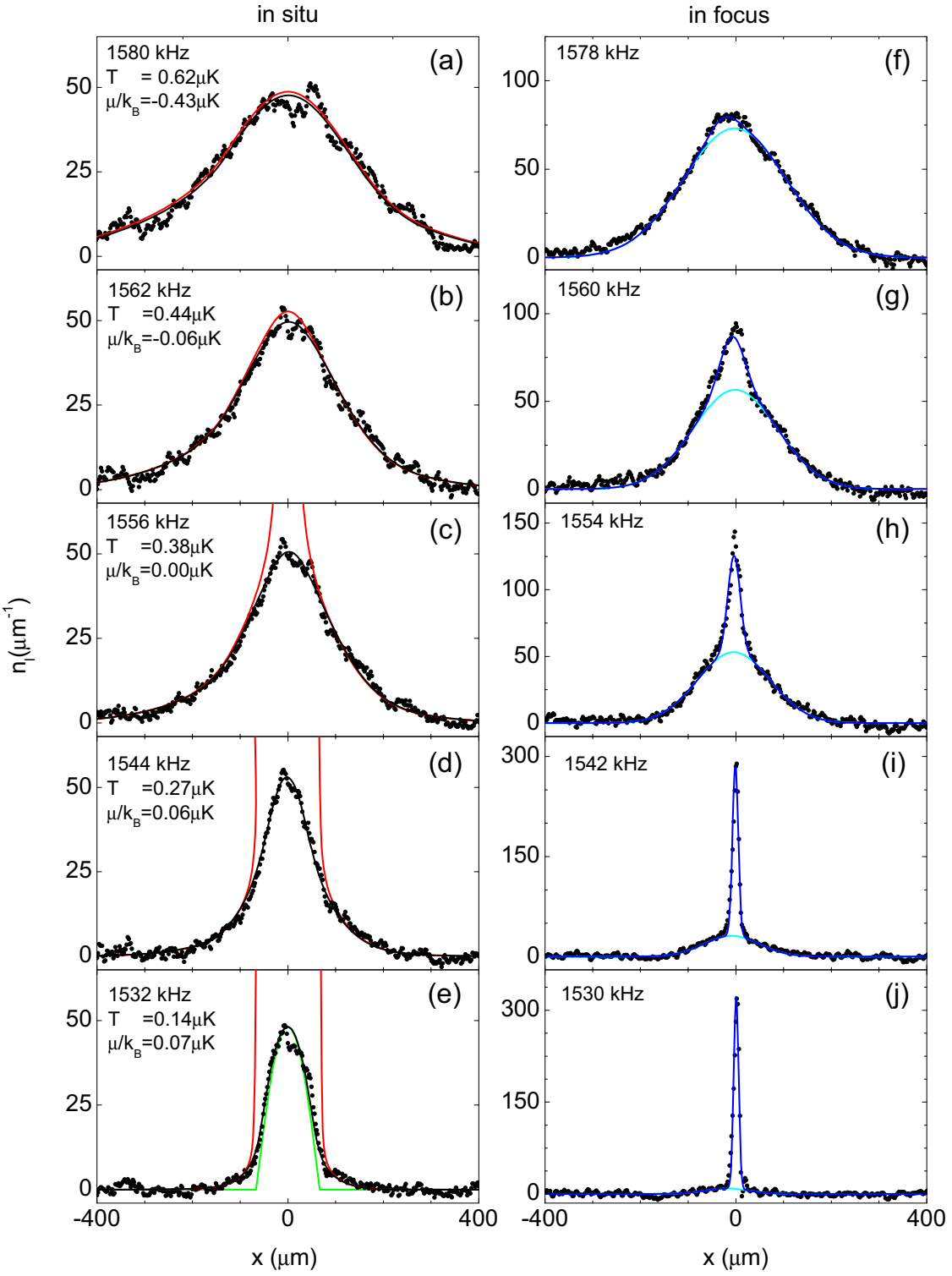

Figure 6.1: Linear atomic density from absorption images obtained *in situ* (a)-(e) and *in focus* (f)-(j).

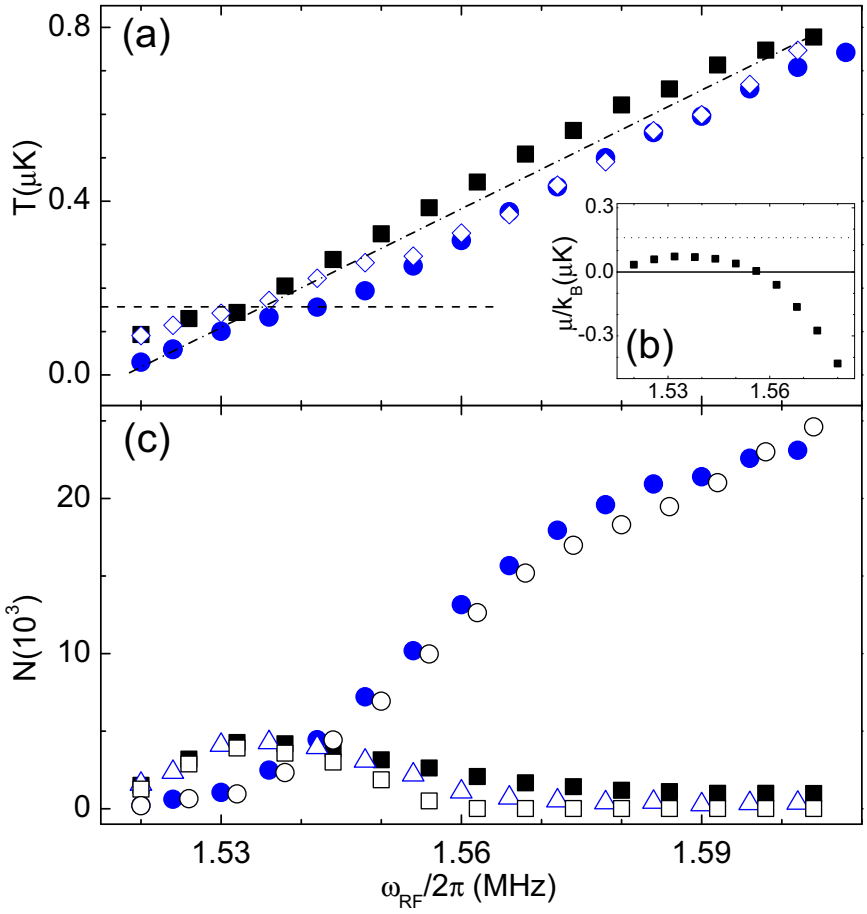

Figure 6.2: Characterization of the measured atomic clouds as a function of the final RF frequency ω_{RF}, as determined from fits of the Yang-Yang model to the *in situ* data and Gaussian fits to the *in focus* data. (a) Temperature from the *in situ* data (■) and from the radial (◇) and axial (●) size of the broad Gaussian fit to the *in focus* data. The dash-dotted line is to guide the eye and indicates a ratio of 11 of the trap depth (set by ω_{RF}) and the cloud temperature. The dashed line corresponds to $\hbar\omega_\perp/k_B$. (b) Chemical potential from the Yang-Yang fit. The dashed line indicates $\hbar\omega_\perp/k_B$. (c) Atom number from the *in focus* data: wide distribution (●) and central peak (△); from the Yang-Yang model fit to the *in situ* data: atoms in the radial ground state (■), in radially excited states (○), and atoms in the radial ground state experiencing $\mu(x) > 0$ (□).